
# LeakyScatter: A Frequency-Agile Directional Backscatter Network Above 100 GHz

Atsutse Kludze and Yasaman Ghasempour, *Princeton University*

https://www.usenix.org/conference/nsdi23/presentation/kludze

This paper is included in the
Proceedings of the 20th USENIX Symposium on
Networked Systems Design and Implementation.

April 17–19, 2023 • Boston, MA, USA

978-1-939133-33-5

Open access to the Proceedings of the
20th USENIX Symposium on Networked
Systems Design and Implementation
is sponsored by

جامعة الملك عبدالله
للعلوم والتقنية
King Abdullah University of
Science and Technology

# LeakyScatter: A Frequency-Agile Directional Backscatter Network Above 100 GHz

Atsutse Kludze and Yasaman Ghasempour
*Princeton University*

## Abstract

Wireless backscattering has been deemed suitable for various emerging energy-constrained applications given its low-power architectures. Although existing backscatter nodes often operate at sub-6 GHz frequency bands, moving to the sub-THz bands offers significant advantages in scaling low-power connectivity to dense user populations; as concurrent transmissions can be separated in both spectral and spatial domains given the large swath of available bandwidth and laser-shaped beam directionality in this frequency regime. However, the power consumption and complexity of wireless devices increase significantly with frequency. In this paper, we present *LeakyScatter*, the first backscatter system that enables directional, low-power, and frequency-agile wireless links *above 100 GHz*. LeakyScatter departs from conventional backscatter designs and introduces a novel architecture that relies on aperture reciprocity in leaky-wave devices. We have fabricated LeakyScatter and evaluated its performance through extensive simulations and over-the-air experiments. Our results demonstrate a scalable wireless link above 100 GHz that is retrodirective and operates at a large bandwidth (tens of GHz) and ultra-low-power (zero power consumed for directional steering and $\leq$ 1 mW for data modulation).

## 1 Introduction

Low power communication has become increasingly important in emerging applications such as home automation, smart healthcare, high-quality video streaming, and localization [22, 44, 57, 58]. The number of low-power wireless devices is expected to grow to 41 billion by 2025 [36]. While the last few years have seen rapid innovations in the design and implementation of low-power wireless communication [17, 25, 29, 33, 40, 62], existing networks are limited in the number of nodes that they can concurrently support [10, 31].

The use of frequencies above 100 GHz (henceforth referred to as the terahertz (THz) band) provides unique opportunities for concurrent transmissions. First, the availability of a large swath of spectrum above 100 GHz will facilitate dense user populations to operate concurrently at orthogonal frequency channels. Second, narrow-beam directional transmission and reception, which is required to combat the high path loss in this regime, provides additional opportunities for simultaneous transmission through space division multiple access. The sub-THz frequencies offer the best of the RF and Optical spectrum: like RF, they can be phase modulated and experience lower penetration and reflection losses when compared to optical while still providing a large swath of continuous bandwidth and laser-shaped beams. Indeed, these properties have made THz frequencies promising for 6G wireless technology. Despite these advantages, operation at such a high frequency is fundamentally power demanding since the power consumption of the RF circuitry is proportional to the frequency. This high power consumption has even stalled the deployment of mobile 28 GHz nodes and will worsen at the THz regime [8, 46–48, 52]. Furthermore, creating directional beams requires large antenna arrays, drastically increasing the power consumption and complexity of the device. This challenge worsens under mobility when constant beam adaption is needed to maintain the link. For these challenges, most existing low-power solutions have been limited to sub-6 GHz bands [35, 45, 54], with a few recent narrow-band demonstrations at 24 GHz band [30, 37, 53].

In this paper, we present *Terahertz Leaky-Waveguide Backscatter (LeakyScatter), a novel architecture for frequency-agile directional backscattering above 100 GHz*. Instead of generating and emitting THz signals, LeakyScatter piggybacks its data on the impinging THz signals that are emitted from a THz transceiver. To enable directional connectivity, we exploit the unique properties of leaky-wave antennas. Leaky-wave antennas are traveling wave structures that can be realized with metal waveguides or on CMOS. In its simplest form, a leaky-wave antenna is a parallel-plate metal waveguide having open slit(s) on one side, with the interesting characteristic that guided waves (inside the waveguide) can *leak out* into free space such that the emission

angle is correlated with the frequency of the signal [21]. These frequency-dependent radiations have been recently exploited for THz path discovery and localization [12, 13, 28] and have also been demonstrated in CMOS technology [50]. In this paper, we leverage angle-frequency coupling in leaky waveguides to enable the *first* passive ultra-wideband and retrodirective structure above 100 GHz.

Our key insight is that leaky waveguides are reciprocal devices, i.e., its reception characteristics are identical to its transmission's. When it acts as a receiver, the impinging signals couple into the waveguide only if their spectral content is in agreement with the incident angle (i.e., where the angle of emission and reception from the waveguide is frequency-dependent). Hence, we devise two symmetrical slits in LeakyScatter: one for accepting free-space ambient signals into the waveguide, and the other for leaking those signals back into the air. Specifically, a far-field active transceiver emits a THz signal toward the LeakyScatter. The impinging signal would then couple into the waveguide where it is guided toward the second slit and radiates out back to free-space forming a directional beam that points to the transceiver's location, thereby enabling retrodirectivity. We emphasize that our retrodirective structure is truly wideband and spectrally agile as LeakyScatter can operate between 100 GHz and 500+ GHz. Further, the directionality is achieved with zero power consumption. The active transceiver, however, is expected to be power demanding as it is capable of generating tunable wideband signals and steering them to any desired direction. Note that the discrepancy in RF capabilities between active transceivers and low-power nodes is often the case in backscatter wireless networks.[1]

In LeakyScatter, we enable data transmission by modulating the amplitude of the THz backscattered signal.[2] Our key observation is that the size of the slit directly impacts the amount of coupling efficiency (or backscatter power). Yet, the physical dimension of the slits in leaky antennas are fixed upon production; instead, we control the *effective size* of the aperture by re-configuring the trajectory of guided waves inside LeakyScatter's waveguide. In particular, we employ an mm-sized electrostatic MEMS mirror inside the waveguide's cavity to dynamically and electronically guide EM signals toward the slit or steer them away from it, as shown in Fig. 1. We characterize the backscattered power as a function of the micro-mirror's orientation using ray optics principles. We then optimize the architecture of LeakyScatter for maximum link budget and modulation order.

We fabricate a custom LeakyScatter and deploy it together with our in-house THz transceiver. We present the *first experimental exploration of wireless backscattering above 100 GHz*. We evaluate the performance of LeakyScatter with extensive COMSOL simulations and experiments in various settings. We experimentally validate the reciprocity in leaky-wave devices, and characterize the retrodirective beams that radiate from our LeakyScatter nodes. Finally, we demonstrate low-power amplitude modulation and evaluate the feasibility of concurrent THz backscatter links in dense LeakyScatter networks.

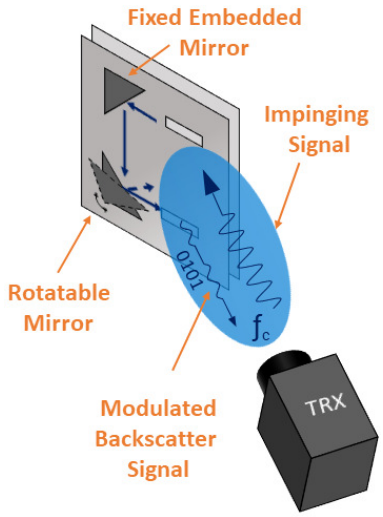


Figure 1: Illustrating the retrodirective backscatter link between our LeakyScatter and a broadband transceiver.

## 2 Background and Related Work

### 2.1 Wireless Backscatter Communication

Backscatter technology is introduced for energy-efficient communication between power-constrained wireless devices [3, 20]. The underlying idea is to allow low-power nodes to piggyback their data on an ambient signal instead of generating their own RF signal, which would demand power-hungry components such as mixers, oscillators, and amplifiers [34]. In particular, an access point (AP) transmits an RF signal to the node which will then be modulated and reflected back to the AP for processing. For example, a simple On-Off Keying (OOK) can be implemented where reflecting the AP's signal translates to sending a '1' bit and absorbing the signal represents the '0' bit.

Recently, there has been significant work on extending the communication range [9, 23, 41, 56] and improving the data rate of backscatter communication links [26, 30]. In particular, employing low-power coding techniques such as chirp spread spectrum has shown promise for decoding backscattering signals below the noise floor [6]. However, while these techniques can achieve long-range communications, they often do not scale well with the number of devices, i.e.,

[1] In this work, we only focus on the backscatter architecture. Designing efficient high-frequency transceiver is an active field of research and is beyond the scope of this paper.

[2] We emphasize that noncoherent on–off keying is identified as one of the two modes in the first standardization of sub-THz bands by the IEEE 802.15.3d task group [42].

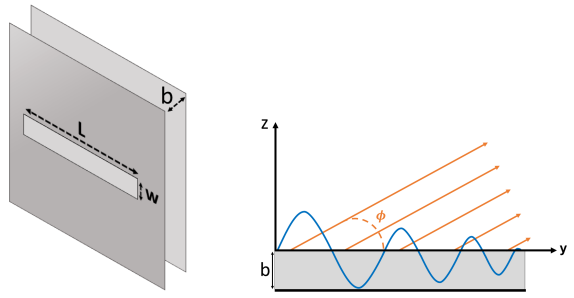


(a) (b)

Figure 2: Parallel plate leaky waveguide: (a) front view (b) side view.

they are often limited to very few (1-2) concurrent links. The state-of the-art protocol (NetScatter [18]) allows for concurrent transmission of 256 backscatter devices over a bandwidth of 500 KHz. NetScatter relies on the ability of the low-power nodes to generate cyclic shifted chirps, which is relatively power-demanding. Further, the number of concurrent users is inherently bounded to the bandwidth and the spectral resolution at endpoint devices.

Instead, in this paper, we take a fundamentally new approach to backscattering and introduce a spectrally-agile and retrodirective node architecture that scales the number of concurrent users through the division of signals in frequency and space. In this context, moving to higher frequencies is advantageous for two reasons: *(i)* the large availability of bandwidth allows for serving more concurrent users on non-overlapping channels; and *(ii)* directional communication (required for mmWave and THz links) provides opportunities for concurrent transmission of nodes that are sufficiently separated in space.

Therefore, unlike traditional backscatter nodes that operate below 6 GHz, our backscatter architecture aims at establishing backscatter links above 100 GHz. A few recent works have demonstrated retrodirective backscattering at mmWave bands (up to 28 GHz) using the Van Atta technique [19, 30, 37, 53]. Unfortunately, Van Atta Arrays are inherently narrow-band as the transmission lines are optimized at a particular wavelength, which is fixed (non-configurable) after fabrication.

## 2.2 Leaky-Wave Antennas

Leaky Wave Antennas (LWAs) belong to the general class of traveling wave antennas that can be implemented with circuits [50] or simply with an air-filled parallel-plate waveguides with an open slit on one of the plates [2]. A traveling wave inside the waveguide may *"leak"* into free-space through the open slit, as depicted in Fig. 2. Notably, Maxwell's equations and the boundary condition suggest that the direction of emission from the slit is correlated with the frequency of the guided wave. By assuming infinitely thin metal plates that are infinitely conductive, the phase matching conditions for the $TE_1$ mode yields [24]:

$$\phi(f) = asin\left(\frac{c}{2bf}\right), \tag{1}$$

where $\phi$ is the emission angle ( relative to the waveguide plate), $f$ is the frequency of the input signal, $b$ is the plate separation, and $c$ is the free-space speed of light. Eq. (1) indicates that signals with higher frequencies emit out at lower azimuth angles and vice versa.

While Eq. (1) captures the optimal emission angle as a function of frequency, in practice, the signals leaking from the waveguide can appear at a range of angles, albeit encountering different coupling losses. To understand this broader angular width, we can treat the leaky waveguide slot as a finite-length aperture, which produces a diffraction pattern in the far-field. According to Huygen's principle [15, 55], for a diffracting aperture (i.e., slot length) of L and the dominant $TE_1$ mode, the far-field radiation pattern can be written as

$$\begin{aligned} G(\phi, f) &\propto \int_{-L/2}^{L/2} e^{-j\beta_y y} e^{-\alpha y} e^{jk_0 cos(\phi) y} dy \\ &= sinc\left((\beta_y - j\alpha - k_0 cos\phi)\frac{L}{2}\right), \end{aligned} \tag{2}$$

where $sinc(x) = sin(x)/x$, $k_0 = \omega/c$ is the free-space wave-number, $\alpha$ is the leakage attenuation, and $\beta_y$ is the propagation constant. $\beta_y$ can be written as $\beta_y = \sqrt{k_0^2 - (\pi/b)^2}$ when the parallel-plate waveguide has an air core. Eq. (2) also confirms the dependency of emission pattern on frequency where the peak output radiation occurs at the angle at which $Re\{(\beta_z - j\alpha - k_0 cos\phi)\frac{L}{2}\} = 0$, yielding Eq. (1). It should be noted that the coupling efficiency and reception behavior of a leaky-wave antenna are independent of polarization [43].

Recently, leaky-wave antennas have been used in multiple sensing tasks including link discovery [12, 14], mobility tracking [13], 3D localization [28], physical-layer security [61], and even for wireless authentication [27]. However, this paper is the first work toward exploiting the angle-frequency relation and the antenna reciprocity for frequency-agile backscattering.

# 3 Design

In this section, we describe the underlying principles and key components of LeakyScatter.

## 3.1 Design Overview

The large amount of available bandwidth above 100 GHz together with directional transmission opens up opportunities for concurrent high-rate networks beyond 5G. Yet, operation at such high frequencies is fundamentally power-demanding since the power consumption of the RF circuitry is

proportional to the frequency. Further, creating directional beams would require large antenna arrays, which itself increases the power and complexity. Previously-established backscattering technology addresses the first challenge by allowing nodes to piggyback their data on an ambient signal instead of generating their own RF signal, thereby, eliminating the need for power hungry components. However, existing backscatter designs are either directional and narrow-band [30, 37, 53] or omnidirectional at much lower frequency bands (e.g., sub-6 GHz) [35, 45, 54].

Our proposed LeakyScatter is the first frequency-agile directional backscattering network at THz bands. Instead of conventional systems that use phased array antennas for beam steering, we introduce a fundamentally novel node architecture based on leaky-wave antennas. Our key observation is that a leaky wave antenna is inherently reciprocal. In particular, the first-principle model suggests that the frequency-dependent radiation in leaky-wave antennas is identical in both transmission mode (guided signals coupling out into free-space) and reception mode (free-space waves coupling into the waveguide). We leverage this interesting characteristic to build a fully-passive retrodirective node. We design a two-slit waveguide (one for receiving signals from the transceiver (TRX) and another for transmitting the signal back directionally toward the transceiver), as shown in Fig. 1. We also embed two mm-sized mirrors inside the waveguide to guide the propagation path between the two apertures.

Given the angle-frequency relationship, the TRX should choose the *correct* frequency to communicate with LeakyScatter nodes depending on the node location and orientation relative to TRX. Fortunately, single-shot angular localization with leaky-wave antennas has been successfully demonstrated in the literature [28]. Here, we assume that the TRX can localize all LeakyScatters by implementing such prior schemes. Further, we assume that the TRX has flexible ultra-wideband transmission and detection capabilities. Such asymmetry between the RF capabilities at the TRX and low-power nodes is typical in all backscatter networks.

In order to piggyback information bits on backscattered signals, we enable amplitude modulation by changing the trajectory of in-coupled waves. Specifically, a small rotation in one of the embedded mirrors would cause significant fluctuations in the amount of power leaked into free-space. Hence, we realize amplitude modulation by dynamically changing the voltage of a MEMS mirror according to the bit stream. We discuss other potential modulation strategies in Sec. 6. Finally, we emphasize that LeakyScatter is ultra-wideband (supporting bandwidths upto few 10s of GHz) and frequency-agile (supporting carrier frequencies from 100 GHz to 500 GHz), retrodirective, and scalable to large-scale networks. Next, we will illustrate the key components of LeakyScatter in detail.

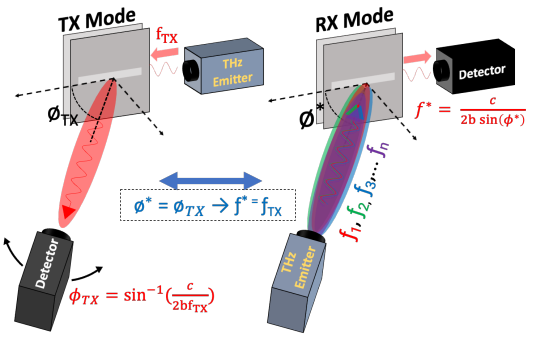


Figure 3: Illustration of reciprocity in leaky waveguide: the angle frequency coupling holds in both transmission and reception modes.

## 3.2 Retrodirectivity in LeakyScatter

The retrodirectivity in LeakyScatter is rooted in the antenna reciprocity of leaky-wave antennas. First, we formally model this reciprocity. Consider a tunable source, a broadband detector, and a single-slit waveguide as shown in Fig. 3. First, the tunable source excites the waveguide (TE1 mode) with a signal at frequency of $f_{TX}$. Given the angular-frequency coupling, the waveguide will act as a directional transmitter creating a directional beam in the far-field (labeled as TX mode in Fig. 3). The detector then measures the received power at various angles to estimate the radiation pattern of the leaked waves. Eq. (1) suggests a direct one-to-one relationship between the angle at which maximum power is received (denoted as $\phi_{TX}$ in Fig. 3) and $f_{TX}$. Next, we swap the detector and source while keeping the same waveguide. The source emits out signals at different frequencies ($f_1, f_2, ..., f_N$) while the broadband detector captures the power of coupled waves at each corresponding frequency. Antenna reciprocity suggests that given a fixed leaky-antenna structure (e.g., aperture size and plate separation), and waveguide positioning (i.e., $\phi^* = \phi_{tx}$), the maximum coupling happens when $f^* = f_{TX}$, which is equal to $\frac{c}{2bsin(\phi_{tx})}$, according to Eq. (1). We will experimentally evaluate this in Sec. 5.

LeakyScatter utilizes two symmetrical apertures, one meant for reception and another meant for transmission. Embedded within the waveguide cavity are two mirrors as illustrated in Fig. 4 to passively redirect the in-coupled signal from the receiving aperture toward the transmitting aperture. More specifically, a THz signal impinging on LeakyScatter at angle $\theta_{TX}$ interacts with the first mirror inside the cavity, which results in a 90° rotation in the propagation direction. Upon impinging on the second embedded mirror, the signal deflects in the reverse direction and moves towards the second slit. The signal then leaks out into free-space through the second slit with an emission angle of $\theta_{RX}$. Given the reciprocity, we have $\theta_{TX} = \theta_{RX}$, as also illustrated in Fig. 4. Such retrodirectivity is essential to our backscatter networks as a single active

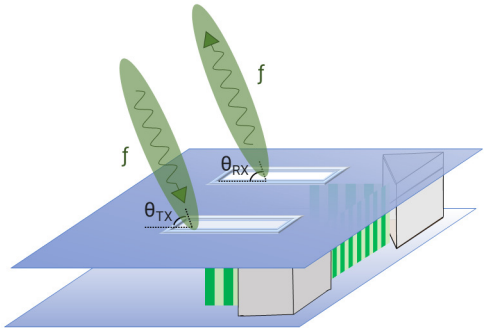


Figure 4: A schematic of LeakyScatter, showing two open slits and embedded mm-sized mirrors to guide the THz waves in between.

transceiver (co-located emitter and detector) is now able to establish a directional link with a truly passive architecture.

We can model the amount of backscattered power by incorporating internal waveguide losses as well as the far-field pattern of LeakyScatter in both TX and RX modes. Specifically, when a transceiver sends an unmodulated signal towards the waveguide, the total power that couples into the waveguide is a function of frequency, $f$, and the impinging angle $\theta_{TRX}$, and can be modeled by Eq. (2). Once the impinging signals couple into LeakyScatter, they will experience propagation losses within the waveguide en route to the transmitting aperture. Finally, the waves emit out with a similar far-field behavior. Therefore, the total backscattered power ($P_{bsc}$) at frequency $f$ can be modeled as:

$$P_{bsc}(f,\phi_{TRX}) \propto G^2(f,\phi_{TRX}) \times (\frac{1}{L_{WG}}), \tag{3}$$

where $L_{WG}$ represents the incurred losses in the guided mode, $\phi_{TRX}$ is the relative angle between the transceiver and the LeakyScatter device. $G(f,\phi_{TRX})$ is defined in Eq. (2). We can see that the maximum backscattering power is achieved when the impinging angle and signal's frequency satisfies $Re\{(\beta_z - j\alpha - kcos\theta)\frac{L}{2}\} = 0$. Next, we explain how $L_{WG}$ is modulated based on the data bit stream.

### 3.3 Data Modulation and Demodulation

So far we have explained how LeakyScatter realizes a retrodirective communication link with an active external transceiver. Now, we explain how LeakyScatter modulates the backscattered signal to transmit information bits. Our design is based on amplitude modulation such that different backscattered power levels translate to distinct sequences of bits. Fluctuation in power level is achieved by an on-demand modification to the power loss inside the waveguide. In particular, one of the aforementioned embedded mirrors is replaced with a mm-sized rotatable MEMS mirror. By changing the mirror's orientation, we seek to control the amount of power that is guided toward the second slit and hence can potentially leak out back to free-space.

Fig. 5 explains how a slight misalignment in the orientation of the MEMS mirror yields a non-negligible drop in the backscatter power. In principle, if the dispersion was minimal and the slit was infinitely thin, even an arbitrarily small rotation of the mirror (i.e., $\delta\theta_{rot}$) could cause zero backscattered power as the guided waves would just miss the open slit. However, in practice, due to dispersion and non-zero slit width, changing the propagation path of guided waves would yield a drop in power. The exact amount of power drop is a complicated function of the frequency, slit dimension, wave propagation constant, the leakage attenuation factor (denoted as $\beta$ and $\alpha$ in Eq. (2)), and more importantly, the amount of rotation (i.e., $\theta_{rot}$).

Our key insight is that the amount of radiated power is proportional to the leakage area and changing the trajectory of guided waves would impact the effective aperture. For simplicity, we consider a rectangular slit (width of $W$ and length of $L$) and assume that signal leakage is uniform across the slit length. As shown in Fig. 5, when $\theta_{rot}$ increases and the guided waves are further directed away from the open slit, the effective aperture area seen by the guided waves should decrease. Using ray optics, we write a first-order approximation of the internal waveguide losses as:

$$L_{WG}(\theta_{rot}) = c_1 + c_2 \frac{A_{slit}}{A_{eff}(\theta_{rot})} = c_1 + c_2 |\frac{2L}{W}\, tan(2\theta_{rot})|, \tag{4}$$

where $c_1$ represents the constant losses such as propagation loss within LeakyScatter and $c_2$ is a constant aperture coupling loss. $A_{slit}$ is the area of the slit and $A_{eff}$ is the effective aperture at rotation angle $\theta_{rot}$. Note that $c_1$ and $c_2$ is a deterministic function of the waveguide geometry (e.g., the internal path length between the two slits) and can be measured and known upon production. Clearly, $L_{WG}$ is minimum at $\theta_{rot} = 0$ and increases with $\theta_{rot}$. Combining

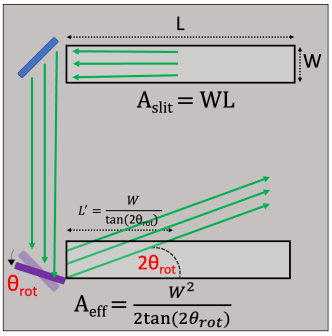


Figure 5: An electronically rotatable mm-sized mirror embedded within LeakyScatter changes the propagation path of guided waves and thus effectively controls the size of transmitting aperture seen by the guided waves.

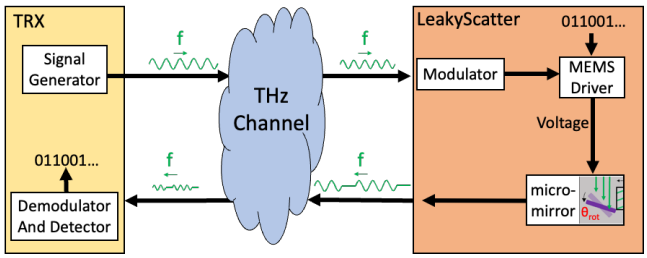


Figure 6: The block diagram of a THz backscatter network.

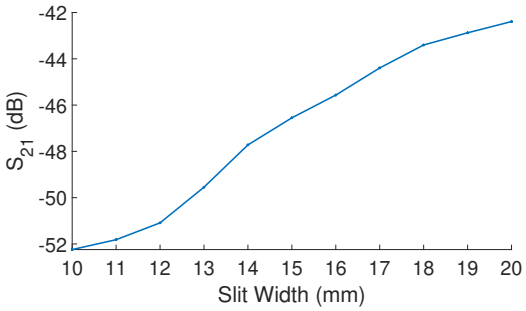


Figure 7: The impact of slit width on total backscatter gain in LeakyScatter.

Eq. (4) and Eq. (3), we can write:

$$P_{bsc}(f) \propto \frac{G^2(f,\phi_{TRX})}{c_1 + c_2|\frac{2L}{W}tan(2\theta_{rot})|} \quad (5)$$

Putting all pieces together, Fig. 6 depicts the block diagram of an TRX-LeakyScatter link. As shown, the modulator at LeakyScatter sets the voltage values at the micro-mirror MEMS driver according to the bit stream. The orientation of the mirror would then change the trajectory of guided waves imposing amplitude modulations. The modulated signal is steered back toward the TRX. At the TRX, the demodulation block retrieves the data bits from analyzing the measured power spectrum.

## 3.4 Design Optimization for Maximizing Reflection Gain

Given the link budget scarcity in backscatter networks, we aim to maximize reflection gain (i.e., backscatter power) in LeakyScatter. Here, we introduce the underlying optimizations and trade-offs that achieve this goal.

### 3.4.1 Slit Geometry

The slit geometry plays a key role in the coupling efficiency and directivity gain in LeakyScatter. In principle, a wider slit is desirable as it allows for a better coupling between guided waves and free-space waves. Yet, the angle-frequency relation in leaky-wave antennas only holds for very thin slits. Indeed, widening the aperture of a rectangular slit quickly

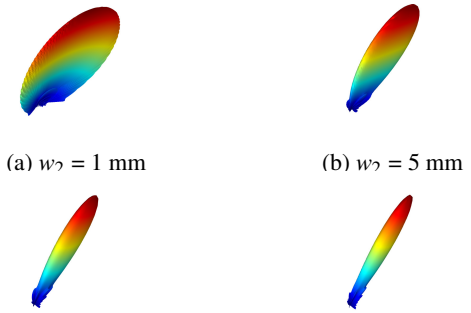

(a) $w_2$ = 1 mm (b) $w_2$ = 5 mm

(c) $w_2$ = 10 mm (d) $w_2$ = 15 mm

Figure 8: Far field emission pattern at various slit widths, showing higher directivity gains achieved with wider slits.

invalidates the monotonic angle-frequency coupling due to the increasingly non-uniform electric field distribution along the slit. To circumvent this issue, we employ trapezoidal apertures (also explored in [16]) to increase aperture size while maintaining the coupling relations. Such slits enable us to increase the captured energy from the receiving slit as well as the out-coupled energy that leaks back out into space. Larger slits also yield smaller diffraction, thus, ray optics models are more accurate with larger slits.

We have simulated LeakyScatter with two symmetric trapezoid slits with varying slit width. Fig. 7 presents the simulated $S_{21}$ parameter against slit widths. The smaller width of these trapezoid-shaped slits is set at $w_1 = 1$ mm while the larger width is varied from $w_2 = 10$ mm to 20 mm in COMSOL. These results were presented in the form of S-parameters, which is a metric to describe the energy propagation across different input/output ports. Here, we define $S_{21}$ as the ratio between the reflected energy from a LeakyScatter compared to incident energy. Hence, $S_{21}$ is a good representative of the backscattering gain. It should be noted that the $S_{21}$ values do not directly translate to the real-world measurements; yet, the general trend can be successfully predicted by analyzing S-parameters.

From Fig. 7, we observe a clear rise in the radiated output power (by 10dB) above its initial starting point at 10 mm. We also look into these simulations in the angular space and plot the directional far-field pattern of the backscattered signal in Fig. 8. As shown, the beams become more pencil-shaped and narrow, leading to higher directivity gains. Therefore, from both simulations, we expect a higher link budget with wider trapezoid slits. However, we emphasize an important tradeoff here: intuitively, with a wider aperture, imposing a fixed power/amplitude fluctuation of $P$ would require a greater mirror rotation angle ($\theta_{rot}$). Unfortunately, our embedded MEMS mirrors are extremely small (mm-sized) and thus limited in their maximum rotation angle (e.g., 5° in our setup). Further, in amplitude shift keying (ASK), the number of symbols (or modulation order) depends on our flexibility to

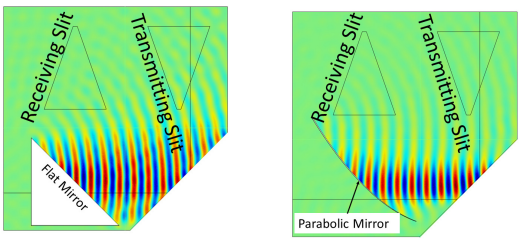


(a) (b)

Figure 9: E-Field simulation of (a) a flat mirror and (b) an off-axis parabolic mirror showing the impact of mirror geometry on dispersion inside the waveguide.

create sufficiently distinct amplitude levels. Hence, we argue that thinner slits are more sensitive to small mirror rotations, so they support higher modulation orders. We carefully take into account the two sides of this tradeoff and fabricate LeakyScatter with the optimal slit width of $w_2 = 15$ mm.

### 3.4.2 Parabolic Mirror vs. Flat Mirror

The fixed mirror in LeakyScatter provides a 90-degree rotation in the trajectory of guided waves. The guided waves dispense as they travel inside the waveguide demanding a large electronically-controlled mirror to collect and rotate these waves. In order to keep the mirror size to mm-scale, we explore other possibilities for the fixed mirror. In particular, unlike flat mirrors, parabolic mirrors can focus EM radiation to a focal point. Hence, we use an 90° Off-Axis-Parabolic (OAP) mirror instead of a flat mirror to decrease dispersion in LeakyScatter. An OAP mirror is a segmented part of a parabolic mirror that diverts the incident signal by a specific angle while focusing it at the same time.

Fig. 9 illustrates the simulation results of our OAP mirror in comparison with a flat reflected surface at 173 GHz. This plot demonstrates the E-field magnitude only between the two mirrors to highlight the impact of the mirror shape. While the flat mirror successfully reflects the incident wave, it causes outward radiations as opposed to the parabolic mirror that focuses the beam to the center of the MEMS mirror. LeakyScatter thus takes advantage of an OAP mirror to accurately re-direct guided waves toward the transmitting slit and thereby increase the output power.

## 3.5 Concurrent Backscatter Links

The directional and wideband operation in LeakyScatter networks allows for multi-node concurrent transmissions. In particular, LeakyScatter supports a wide range of frequencies (e.g., from 100 GHz to 500 GHz). Albeit, the correct spectral band should be selected based on the angular configuration of LeakyScatter relative to the active TRX. When multiple LeakyScatter devices are sufficiently separated in the angular

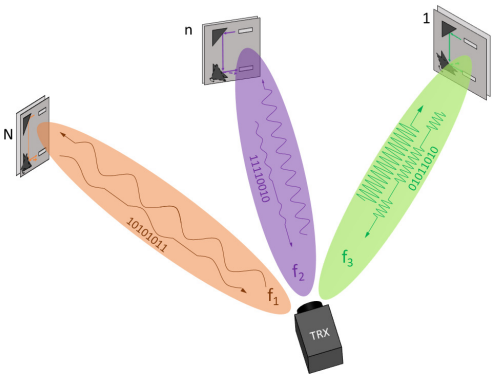


Figure 10: Concurrent transmissions of multiple LeakyScatter devices where backscattered signals can be separated in spatial and/or spectral space.

domain, they can simultaneously and independently modulate a different sub-band of the ambient wideband spectrum. This separation in the angular domain can be seen with distributed nodes at different locations around the TRX (as shown in Fig. 10) or even in co-located nodes that have different orientations. A straightforward strategy is to make TRX broadcast a pseudo-pulse in all directions to collect data from all existing nodes.[3] In such a case, spatially-separated LeakyScatters will modulate different sub-bands; thus, a simple power detection across spectrum can retrieve the information of multiple backscatter nodes. We emphasize that such a scheme relies solely on power measurements. Each LeakyScatter initiates its packet with a pre-known preamble that is utilized at TRX for node identification, localization, and steady-state power calibrations.

Interestingly, the bandwidth of a backscatter link would also depend on the incident angle of THz signals on LeakyScatter. Indeed, the non-linear angle-frequency function causes the in-coupled/out-coupled spectral range (and therefore bandwidth) to also change with angle. Particularly, the operating bandwidth for a receiver located at the far-field of a typical leaky waveguide device at an angle $\phi$ relative to the waveguide can be described by

$$BW(\phi) = \frac{df}{d\beta}\frac{d\beta}{d\phi}\Delta\phi = \frac{c_0}{2b \cdot \sin\phi \tan\phi}\Delta\phi, \qquad (6)$$

where $\Delta\phi$ is the effective angular aperture subtended by the receiver and $\beta$ is the wave number of guided waves.

Eq. (6) indicates that the bandwidth is wider for lower emission angles. Hence, given a fixed application-driven bandwidth per node, a non-uniform distribution of concurrent LeakyScatters is expected across the entire angular space.

In summary, the Thz LeakyScatter networks offer a two-layer protection against inter-user interference. Namely,

[3] Designing efficient medium access protocols for multi-node backscattering is out of the scope of this work and is a subject of future studies.

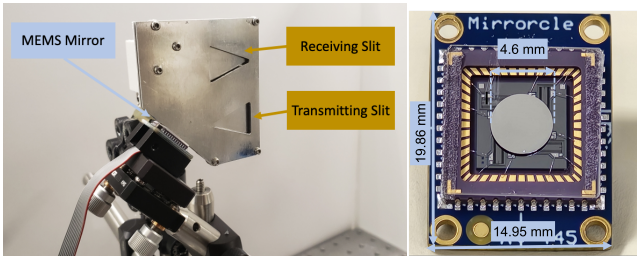


(a) (b)

Figure 11: Our (a) fabricated LeakyScatter with (b) a 4.6 mm electrostatic MEMS mirror.

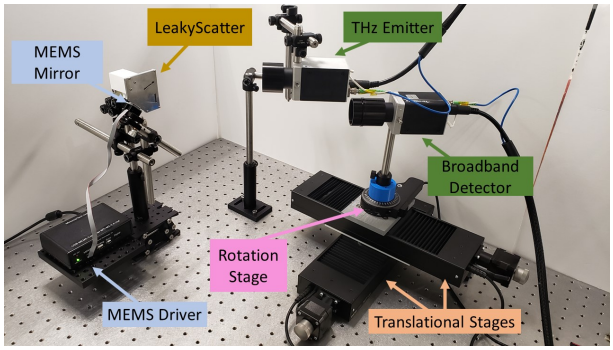


Figure 12: Our experimental setup.

the directionality of the reflected signals offers opportunities for space division multiple access and the inherent spatial-angular correlations allow the leaky-wave backscatter nodes to operate on different sub-bands according to their angular settings. This flexible multi-band operation would be self-regulated by the LeakyScatter's architecture at zero power costs, allowing scalability to dense user populations.

## 4 Experimental Platform and Methodology

We evaluate the performance of our LeakyScatter through extensive COMSOL simulations and over-the-air experiments. Our custom waveguide-based backscatter device, as illustrated in Fig. 11, is constructed with two thin metal plates held in parallel at a separation of 1 mm (i.e., $b = 1$ mm). The overall dimension is 60 mm $\times$ 54 mm. On the front metal plate, we cut two trapezoidal shape slits with longer and shorter widths of 1 mm and 15 mm, respectively. Both slits are 20 mm long. We embed a reflecting OAP mirror that has a smooth metal surface in between the two plates (hence, the thickness of the mirror is also 1 mm). We emphasize that building such a device is cheap (only a few cents) and can be done in a machine shop. To modulate the amplitude of backscattered signals, we employ a mm-sized MEMS mirror, offering continuous rotation in both its x and y directions (with a max rotation angle of $\pm 5^\circ$). The average power consumed by the MEMS mirror is less than 1 mW for continuous full-speed operation. The mirror is controlled via a low-profile driver with max voltage of 5 V. Resonant frequencies of these mirrors range from a few kHz up to tens of kHz and change with mirror size [38].

Our system architecture assumes a tunable wideband transceiver that is able to transmit signals above 100 GHz and steer them toward LeakyScatter nodes. Hence, we use a time-domain broadband system (TeraMetrix T-Ray [1]) that produces an ultra-short pulse with a flat frequency response between 100 GHz to 400 GHz. The detector measures the electric field magnitude at a wide range of frequencies with a spectral resolution of 1.22 GHz (sampling rate of 10 THz). The emitter and detectors are both linearly polarized with a polarization extinction ratio (the ratio of transmitted/received power between the intended and orthogonal polarization modes) $<$ 20:1. We collect raw time-domain samples and apply conventional signal processing techniques (smoothing, filtering, FFT, etc.) to isolate the signal at the spectral range of interest. Note that even though our testbed provides time-domain waveforms, LeakyScatter only uses power measurements (albeit across multiple frequencies) for data demodulation and detection.

Fig. 12 demonstrates our experimental setup consisting of the LeakyScatter and our THz emitter and detector. The emitter is configured at various settings. The detector is placed on a motorized rotation stage on top of a 2D motorized translation stage providing high-precision movement around the waveguide at various configurations. The emitter is equipped with a collimating lens that directs the THz signal into the upper slit of the waveguide.

Our evaluations are limited to an angular range of 20-60 degrees due to our transmitter's low output power. Specifically, the transmit power above 400 GHz, which corresponds to angles below 20 degrees, is always about 6 dB or more weaker, making the reflected signal harder to observe. Additionally, signals are very noisy at $<$ 170 GHz due to a combination of higher dispersion inside the waveguide, getting closer to the cutoff frequency (which is currently 150 GHz but can be changed by modifying the plate separation) and limited spectral resolution of the setup. A higher transmit power is needed to compensate for these losses and will be addressed with future THz transmitters. Nevertheless, we emphasize that our observations and conclusions presented in the paper hold true for all other angles.

## 5 Evaluation

In this section, we discuss our over-the-air experiments and evaluate the key design components of LeakyScatter.

### 5.1 Reciprocity

First, we experimentally characterize and compare the transmission and reception characteristics of leaky

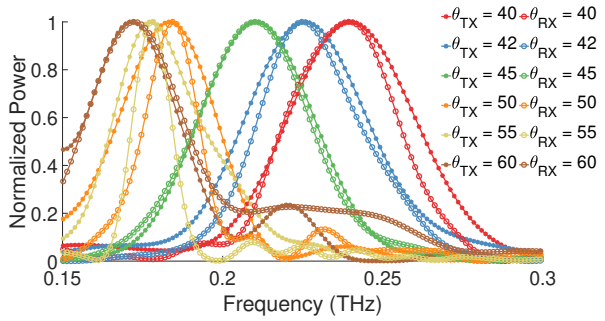


Figure 13: Experimental evaluation of the leaky-wave antenna reciprocity: The angle-frequency correlation holds in both transmission and reception modes.

waveguides to validate the reciprocity in angle frequency coupling. This is a crucial building block for designing a waveguide-based retrodirective backscatter device.

**Setup.** To this end, we employ two different configurations, as also shown in Fig. 3. In particular, for measuring the emission radiation pattern of a leaky-wave antenna, we focus a THz pulse into a single-slit waveguide with an external lens of focal length 75mm. The THz detector is placed on a 2D translation stage at a fixed distance where it can be configured at multiple angle directions relative to the waveguide. Similarly, our setup for measuring the reception pattern of the leaky-waveguide switches the source and the detector, i.e., the wideband source is now placed on a 2D translation stage and the detector focused into the waveguide. In both setups, the same exact waveguide was used. We configured the detector in transmission and source in reception at different angles, each corresponding to $\theta_{RX}$ and $\theta_{TX}$ from Fig. 4 respectively, ranging from 30° to 63°.

Fig. 13 shows the normalized power spectrum measurements from both reception and transmission for a few configurations, namely, 40°, 42°, 45°, 50°, 55°, and 60°. As the angle changes, we see a clear shift in the peak frequency and bandwidth in both modes (reception and transmission), obeying both equations Eq. (2) and Eq. (1). More importantly, the peak frequencies in the reception and transmission modes are in agreement, with the greatest discrepancy being a 2 GHz difference at 60°. There is, however, a discrepancy in the bandwidths of the reception and transmission measurements with the transmission bandwidths being generally larger than the reception. This is largely a result of the different distances of the detector-waveguide in transmission mode (38cm) and of the source-waveguide in reception mode (29.5cm). The shorter distance in transmission allows for a larger acceptable range of in-coupling frequencies, as opposed to the reception setup, and hence a wider bandwidth. Nevertheless, the overall spectral profiles closely follow each other.

*We have experimentally illustrated that leaky-wave antennas are reciprocal, i.e., the angle-frequency relationship holds true when the antenna used in transmission and reception modes. LeakyScatter leverages this property to enable retrodirective scattering with zero power consumption.*

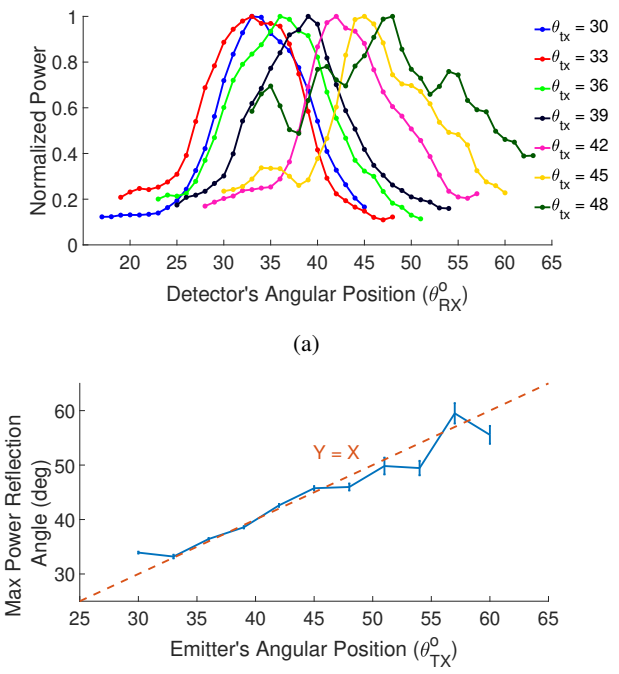


Figure 14: Experimental characterization of retrodirectivity in LeakyScatter: (a) The measured radiation patterns at different settings; (b) the max-power backscatter angle vs. the ground truth impinging angle.

## 5.2 Retrodirectivty

Next, we experimentally evaluate the retrodirectivity in LeakyScatter, which is the ability to steer the backscatter signals toward the transceiver. Such directional communications are essential for closing the link given the high path loss at 100 GHz.

**Setup.** To assess this, we use the setup illustrated in Fig. 12. We integrate a fixed mirror (instead of a rotating mirror) inside the waveguide to direct the guided waves from the receiving aperture toward the transmitting aperture. We try multiple impinging angles between the THz emitter and LeakyScatter ($\theta_{TX}$). Each time, we move the THz detector on a 2D stage to measure the radiation pattern of directional backscatter signals. Recall that given the reciprocal angle-frequency coupling of leaky waveguides, we expect to observe the backscattered signal being strongest when the angle of reflection is the same as the impinging angle.

Fig. 14a presents the normalized power distribution of backscattered signal across space given several THz source configurations ($\theta_{TX}$): 30°, 33°, 36°, 39°, 42°, 45°, and 48°. Given that our source is wideband, evaluation for each of the backscattering transmissions were restricted to spectral band where Eq. (5) gave minimal losses. As expected, in each of

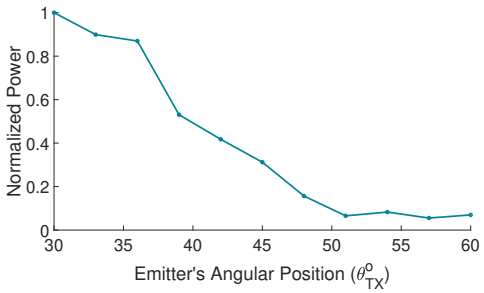


Figure 15: Normalized received power at different reflection angles.

the corresponding curves, the peak reception occurs when the reflection angle is equal to the transmission angle with a half-power beamwidth of 10.56° on average.

Fig. 14b presents these results against the expected behavior demonstrating that LeakyScatter achieves a mean error of 1.911°. We observe an increase in the overall error and fluctuations at higher impinging angles (i.e., when LeakyScatter is placed at larger angles relative to the THz emitter). We find two underlying reasons for this observation: (*i*) the inherent angle-frequency relationship in leaky waveguides is a nonlinear function such that the spectral profile is much more similar (less differential) at larger emission/acceptance angles. This implies that the main lobe of backscatter radiation is prone to slight misalignment when LeakyScatter is positioned at larger angles; and (*ii*) the overall backscattered power is not uniform at different configurations. We show the dependency of maximum reflected power with the angular location of LeakyScatter in Fig. 15. As we approach higher angles, the received power begins to drop (e.g., a drop of 10 dB is observed when the location changes from 30° to 51°). However soon after, the maximum received power begins to be less location-dependent. Although our results show that retrodirective beams can be formed, they also reveal that the directivity gain is not uniform across space. In other words, the amount of reflected power would depend on the LeakyScatter's location relative to the TRX: those positioned at smaller angles have the advantage of forming more directive/high-power backscattered links. This is to some extent a direct impact of our design specs (e.g., OAP mirror) that will be discussed later.

*We have experimentally validated that our proposed backscaterring architecture is retrodirective and can establish and maintain directional connectivity with an external transceiver regardless of its location.*

## 5.3 Data Modulation

Next, we experimentally evaluate the ability of LeakyScatter to modulate the impinging signal for data transmission.

LeakyScatter modulates the reflection path within the waveguide via an electronically-controlled mirror, thus enabling ASK by imposing different reflection power (or amplitude). Specifically, we use the same setup as in 5.2 except that we employ a mm-sized MEMS mirror for digital data encoding. As an example ASK, we map the base orientation of the Mirror ($\theta_{rot} = 0°$) to a "0" bit and the rotation angle of 5 degrees ($\theta_{rot} = 5°$) to a "1" bit. At the detector, different power levels are translated to their corresponding bit. We emphasize that this binary ASK is evaluated as an example scheme. Higher order modulation is feasible with arbitrary encoding of symbols to the embedded mirror's orientation (i.e., reflected amplitude).

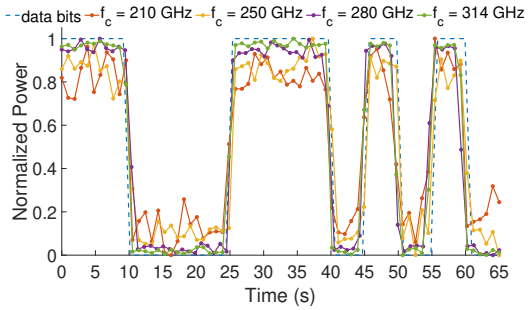


Figure 16: Measured modulated backscattered signal at various center frequencies, showing the spectral agility of LeakyScatter.

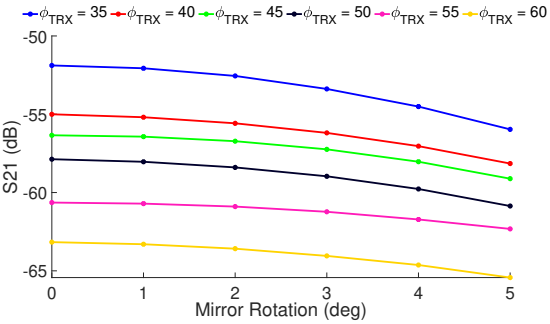


Figure 17: The sensitivity of backscatter gain (captured by $S_{21}$ simulations) to mirror rotation in LeakyScatter.

Fig. 16 shows the successfully transmitted bit stream 0011100010101 with a symbol time of 5 seconds. We repeated this experiment at different center frequencies $f_c$ = *210* GHz, 250 GHz, 280 GHz, and 314 GHz (corresponding to reflection angles of 45°, 37°, 32°, and 28° respectively). Our results demonstrate a successful demodulation/detection regardless of the carrier frequency or LeakyScatter's relative angular location. However, we observe that the difference between the two power levels (representing 0 and 1) gets smaller at lower frequencies. This implies that the ASK modulation order is limited for lower frequencies.

To better understand this experimental observation, we have simulated the LeakyScatter structure in COMSOL and looked into the S-parameters of this device. Specifically, Fig. 17 plots $S_{21}$ as a measure of the backscatter power at different mirror rotations. We repeat the simulations for several impinging angle configurations. Surprisingly, at any mirror orientation, we observe a larger $S_{21}$ at lower impinging/reflecting angles.

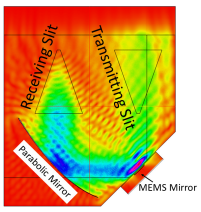


(a) $f_c = 173$ GHz, $\theta_{rot} = 0$

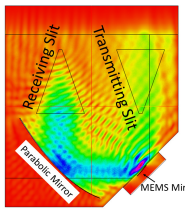


(b) $f_c = 173$ GHz, $\theta_{rot} = 5$

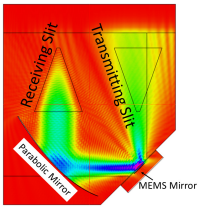


(c) $f_c = 261$ GHz, $\theta_{rot} = 0$

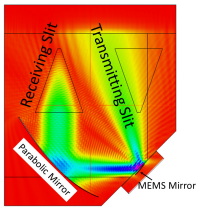


(d) $f_c = 261$ GHz, $\theta_{rot} = 5$

Figure 18: E-field simulations of guided waves in LeakyScatter.

Further, the power drop caused by the mirror's rotation is generally more pronounced at smaller angles (e.g., an $S_{21}$ drop of 2.25 dB at $\theta_{TRX} = 60°$ vs. a 4.1 dB drop at $\theta_{TRX} = 35°$. Note that this trend holds for negative rotations (not shown).

To find the underlying reason, we looked further into the simulated E-field inside the waveguide at the same device configurations. Fig. 18 depicts this with an in-coupled signal of 173 GHz and 261 GHz signal at rotation angles $\theta_{rot} = 0$ and $\theta_{rot} = 5$. Interestingly, we observe less dispersion for the higher frequency tone; i.e., the guided waves are much more directed (laser-like) at 261 GHz, especially as they interact with the embedded parabolic mirror. The propagation path of guided waves can thus be more precisely controlled via a rotating mirror. There is a clear drop in the amount of power at the second (transmitting) slit due to the 5° mirror rotation. This implies that the ASK modulation order (i.e, the number of symbols which here correlate with the number of distinct power levels using an electronically-controlled rotating mirror) is frequency-dependent with higher frequencies offering higher modulation orders.

*We have experimentally demonstrated that we can piggyback information bits on the backscattered signal with LeakyScatter. Interestingly, a higher modulation order can be achieved at higher frequencies due to their small dispersion and laser-like behavior in guided mode.*

## 5.4 Multiple Concurrent LeakyScatters

Finally, we investigate the user capacity in LeakyScatter networks. We consider a single transceiver and emulate multi-node backscattering by placing the LeakyScatter at various locations and collecting the raw power spectrum.

First, we experimentally evaluate the half-power bandwidth at various TRX-LeakyScatter angular configurations. As discussed in Sec. 3.5, we expect larger half-power bandwidths

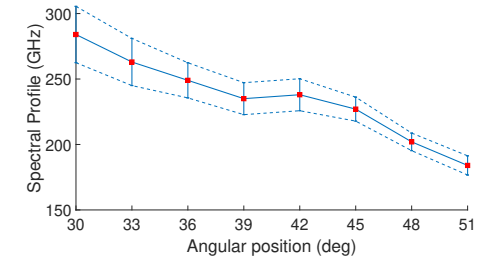


(a)

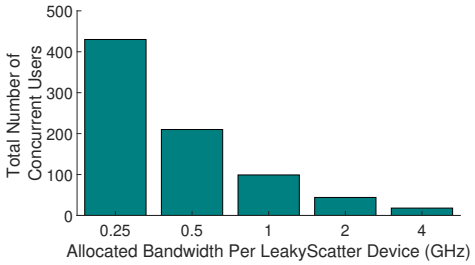


(b)

Figure 19: Experimental characterization of user density: (a) Spectral band of operation in LeakyScatter when configured at various impinging angles; (b) Total concurrent LeakyScatter nodes given their application-driven bandwidth requirements.

at lower incident angles. Fig. 19a confirms this claim through experimental analysis where the bandwidth of backscatter links are captured across different angular positions (all at a fixed distance of 34 cm from LeakyScatter). This observation suggests that the concurrent user capacity ( given a per-user bandwidth) is also non-uniform across space, and dependent on the incident angle with a similar trend.

Fig. 19b shows the emulated total number of concurrent users across the angular domain. We assume directional pencil-shaped beams (1° of beamwidth) at TRX[4]. Further, we emulate five different bandwidths for backscatter communication. Note that in practice, this number is application-dependent. According to Fig. 19b, LeakyScatter can establish 430 simultaneous non-overlapping links with a spectral allocation of 0.25 GHz per user. Similarly, 18 users can be supported at a spectral allocation of 4 GHz each. We emphasize that different backscatter nodes modulate different portions of the spectrum (according to their location and orientation); thereby, having multiple nodes is a simple extension of a single LeakyScatter as the signals are orthogonal in frequency. In the future, we will experimentally implement a multi-backscatter network using a multi-beam multi-frequency emitter.

*We have experimentally demonstrated that by taking advantage of LeakyScatter's retrodirectivity and spectral agility, we can support multiple concurrent backscatter nodes in dense user settings.*

[4]For simplicity, we consider the far-field scenario in which the backscatter range is much larger than the dimension of the physical LeakyScatter nodes.

## 6 Discussion and Limitations

In this section, we discuss the opportunities and limitations in THz backscatter networks as well as our future directions.

**Mobility Support with LeakyScatter.** One of the main challenges in directional communication is maintaining beam alignment despite nodal mobility. LeakyScatter offers a retrodirective link which means the backscatter beam will always point back toward the broadband TRX regardless of device motion. Interestingly, this will be accompanied by a change in the spectral profile observed at the TRX. This opens the door for simultaneous data transmission and localization, an emerging paradigm for 6G wireless systems. Note that leaky-wave antennas have been used recently for angular positing in unmodulated and active settings (non backscattering) [11, 13, 28]. This paper is the *first* effort that exploits the angle-frequency coupling in leaky-wave devices for enabling low-power frequency-agile backscattering at the sub-THz regime.

**Communication Range and Coverage.** A common concern in all backscattering networks is the limited communication range, i.e., the range of a backscatter link is always smaller than an active TX-RX link due to lack of amplification at the backscatter. This issue worsens in sub-THz and THz frequencies that suffer from increased propagation attenuation. Yet, our experimental results demonstrate the feasibility of closing a link at frequencies as high as 314 GHz without any amplifications and via an ultra-low-power broadband emitter/detector. Our source has an average output power of 400 nW across 5 THz non-uniformly. Our current implementation of LeakyScatter, however, has an operating bandwidth of approximately 400 GHz which upon calculation yields a 260 nW average power output. Even under such stringent power budgets, a communication range of half a meter was achieved. This is owed to the directionality at LeakyScatter which compensates for the higher path loss. Note that our communication range is similar to the numbers reported by prior work that uses an active leaky-wave antenna [13, 28] which implies that the limitation in range is a direct result of the employed low-power source and not the architecture of LeakyScatter. Employing more realistic TRX can scale up the transmitter-receiver distance as links at WLAN-scale distances (100+) meters have already been demonstrated above 100 GHz [59, 60].

We note that LeakyScatter is limited in angular coverage of 90°. Prior work proposed a periodic arrangement of slits to extend the coverage of leaky-wave antennas to 180° [32]. To extend the coverage to 360°, open slits on both ends are needed. One potential design is to use three aluminum plates such that two of the plates contain periodic slits and the 'center plate' acts as the common 'back plate'. We will investigate these architectures in the future.

**Fabrication Cost and Power Consumption.** LeakyScatter can be easily fabricated with two thin metal plates, spacers, and an electronically-controlled mirror. Prior work has realized leaky-wave antennas via integrated circuits, i.e., in 65nm CMOS with an area size of $3mm^2$ [50]. The small form factor, ease of fabrication, and low cost make such designs suitable for various IoT applications. The integrated broadband emitter/detector, however, can be power demanding. We emphasize that such asymmetry between the transceiver and the backscatter tag is typical in these networks [34]. Nevertheless, ongoing research continues to develop efficient low-power THz transmitter and detectors suitable for future handheld devices [5, 49, 51].

**Higher Order Modulation.** We have introduced a novel low-power physical layer architecture for THz communication by showing the feasibility of passive THz backscattering; nevertheless, further extensive study is needed for a full-stack demonstration. Additionally, the current achievable data-rates fall behind the speeds promised within the THz regime. The underlying bottleneck is the speed of the electro-static MEMS mirrors which can be addressed through novel modulation strategies. Building high-speed THz modulators is itself an emerging field of research, with recent advances in materials (e.g., carbon nanotubes and graphene) showing promise [4, 7, 39]. In this paper, we consider a noncoherent on–off keying modulation scheme, which is one of the two identified modes in the recent standardization of the IEEE 802.15.3d task group [42]. Nevertheless, in the future, we will explore not only coherent modulation techniques and higher-order amplitude-phase schemes, but also optical modulation techniques, such as via variation in waveguide's electromagnetic permittivity, for larger data-rates.

## 7 Conclusion

In this paper, we present LeakyScatter, a novel structure that enables low-power directional backscattering above 100 GHz. LeakyScatter adopts the inherent dependency of emission angle on frequency in LWAs to passively redirect the signals back in the same direction from which they were transmitted. The proposed architecture utilizes a metal parallel-plate waveguide with two open slits. Data transmission is facilitated via a mm-sized MEMS mirror that modulates the reflection loss (i.e., amplitude of backscattered link) according to the bit stream. Our over-the-air experiments show that LeakyScatter is ultra-wideband and spectrally-agile operating at few 100s of GHz, opening unique opportunities for dense user implementations.

## 8 Acknowledgments

We appreciate the valuable comments and feedback from the anonymous reviewers. This research was supported by the US Air Force, and NSF grants CNS-2145240 and CNS-2148271.

## References


[1] The TeraMetrix T-Ray® 5000 Series Intelligent Terahertz Control Unit. Available at https://lunainc.com/blog/terametrix-t-rayr-5000-series-intelligent-terahertz-control-unit, 2018.

[2] BALANIS, C. A., AND BIRTCHER, C. R. Antenna measurements. *Modern Antenna Handbook* (2008), 977–1033.

[3] BOYER, C., AND ROY, S. Backscatter Communication and RFID: Coding, Energy, and MIMO Analysis. *IEEE Transactions on Communications 62*, 3 (2014), 770–785.

[4] BURDANOVA, M., TSAPENKO, A., SATCO, D., KASHTIBAN, R., MOSLEY, C., MONTI, M., STANIFORTH, M., SLOAN, J., GLADUSH, Y. G., NASIBULIN, A. G., AND LLOYD-HUGHES, J. Efficient Ultrafast THz Modulators Based on Negative Photoconductivity in Controllably Doped Carbon Nanotubes. In *International Conference on Infrared, Millimeter, and Terahertz Waves (IRMMW-THz)* (2019), pp. 1–1.

[5] CHI, T., HUANG, M.-Y., LI, S., AND WANG, H. 17.7 A Packaged 90-to-300GHz Transmitter and 115-to-325GHz Coherent Receiver in CMOS for Full-Band Continuous-wave mm-Wave Hyperspectral Imaging. In *In Proc. of IEEE International Solid- State Circuits Conference (ISSCC)* (2017).

[6] CORREIA, R., DING, Y., DASKALAKIS, S. N., PETRIDIS, P., GOUSSETIS, G., GEORGIADIS, A., AND CARVALHO, N. B. Chirp Based Backscatter Modulation. In *IEEE MTT-S International Microwave Symposium* (2019), pp. 279–282.

[7] DOCHERTY, C. J., STRANKS, S. D., HABISREUTINGER, S. N., JOYCE, H. J., HERZ, L. M., NICHOLAS, R. J., AND JOHNSTON, M. B. An Ultrafast Carbon Nanotube Terahertz Polarisation Modulator. *Journal of Applied Physics 115*, 20 (2014), 203108.

[8] DUTTA, S., BARATI, C. N., RAMIREZ, D., DHANANJAY, A., BUCKWALTER, J. F., AND RANGAN, S. A Case for Digital Beamforming at mmWave. *IEEE Transactions on Wireless Communications 19*, 2 (2019), 756–770.

[9] EID, A., HESTER, J., AND TENTZERIS, M. M. A Scalable High-gain and Large-beamwidth mm-wave Harvesting Approach for 5G-powered IoT. In *IEEE MTT-S International Microwave Symposium* (2019), pp. 1309–1312.

[10] FEDERAL COMMUNICATIONS COMMISSION. The Commission Seeks Comment on Spectrum for the Internet of Things. *ET Docket*, 21-353 (2021).

[11] GHASEMPOUR, Y., AMARASINGHE, Y., YEH, C.-Y., KNIGHTLY, E., AND MITTLEMAN, D. M. Line-of-Sight and Non-Line-of-Sight Links for Dispersive Terahertz Wireless Networks. *APL Photonics 6*, 4 (2021), 041304.

[12] GHASEMPOUR, Y., SHRESTHA, R., CHAROUS, A., KNIGHTLY, E., AND MITTLEMAN, D. M. Single-Shot Link Discovery for Terahertz Wireless Networks. *Nature Communication 11*, 1 (2020), 2017.

[13] GHASEMPOUR, Y., YEH, C.-Y., SHRESTHA, R., AMARASINGHE, Y., MITTLEMAN, D., AND KNIGHTLY, E. W. LeakyTrack: Non-Coherent Single-Antenna Nodal and Environmental Mobility Tracking with a Leaky-Wave Antenna. In *Proc. of ACM SenSys* (2020), pp. 56–68.

[14] GHASEMPOUR, Y., YEH, C.-Y., SHRESTHA, R., MITTLEMAN, D., AND KNIGHTLY, E. Single Shot Single Antenna Path Discovery in THz Networks. In *Proc. of ACM MobiCom* (2020), pp. 317–327.

[15] GROSS, F. B. *Frontiers in Antennas: Next Generation Design & Engineering*. McGraw-Hill Education, 2011.

[16] GUERBOUKHA, H., SHRESTHA, R., NERONHA, J., RYAN, O., HORNBUCKLE, M., FANG, Z., AND MITTLEMAN, D. M. Efficient Leaky-Wave Antenna for Terahertz Wireless Communications. In *Conference on Lasers and Electro-Optics* (2021), Optical Society of America.

[17] GUO, X., SHANGGUAN, L., HE, Y., JING, N., ZHANG, J., JIANG, H., AND LIU, Y. Saiyan: Design and implementation of a low-power demodulator for LoRa backscatter systems. In *Proc. of USENIX NSDI* (Apr. 2022), pp. 437–451.

[18] HESSAR, M., NAJAFI, A., AND GOLLAKOTA, S. NetScatter: Enabling Large-Scale backscatter networks. In *Proc. of USENIX NSDI* (2019), pp. 271–284.

[19] HESTER, J. G., AND TENTZERIS, M. M. A Mm-wave Ultra-long-range Energy-autonomous Printed RFID-enabled Van-atta Wireless Sensor: At the Crossroads of 5G and IoT. In *IEEE MTT-S International Microwave Symposium* (2017), pp. 1557–1560.

[20] ILIE-ZUDOR, E., KEMÉNY, Z., VAN BLOMMESTEIN, F., MONOSTORI, L., AND VAN DER MEULEN, A. A survey of Applications and Requirements of Unique Identification Systems and RFID Techniques. *Computers in Industry 62*, 3 (2011), 227–252.

[21] JACKSON, D. R., AND OLINER, A. A. Leaky-Wave Antennas. *Modern Antenna Handbook* (2008), 325–367.

[22] JAMEEL, F., DUAN, R., CHANG, Z., LILJEMARK, A., RISTANIEMI, T., AND JANTTI, R. Applications of Backscatter Communications for Healthcare Networks. *IEEE Network 33*, 6 (2019), 50–57.

[23] JIANG, J., XU, Z., DANG, F., AND WANG, J. Long-range Ambient LoRa Backscatter with Parallel Decoding. In *Proc. of ACM MobiCom* (2021), pp. 684–696.

[24] KARL, N. J., MCKINNEY, R. W., MONNAI, Y., MENDIS, R., AND MITTLEMAN, D. M. Frequency-division Multiplexing in the Terahertz Range using a Leaky-wave Antenna. *Nature Photonics 9*, 11 (2015), 717.

[25] KELLOGG, B., PARKS, A., GOLLAKOTA, S., SMITH, J. R., AND WETHERALL, D. Wi-Fi Backscatter: Internet Connectivity for RF-powered devices. In *Proc. of ACM SIGCOMM* (2014), pp. 607–618.

[26] KIMIONIS, J., GEORGIADIS, A., DASKALAKIS, S. N., AND TENTZERIS, M. M. A Printed Millimetre-wave Modulator and Antenna Array for Backscatter Communications at Gigabit Data Rates. *Nature Electronics 4*, 6 (2021), 439–446.

[27] KLUDZE, A., AND GHASEMPOUR, Y. Towards Terahertz Wireless Authentication with Unique Aperture Fingerprints using Leaky-Wave Antennas. In *International Conference on Infrared, Millimeter, and Terahertz Waves (IRMMW-THz)* (2022).

[28] KLUDZE, A., SHRESTHA, R., KNIGHTLY, E., MITTLEMAN, D., AND GHASEMPOUR, Y. 3D Localization via a Single Non-Coherent THz Antenna. In *Proc. of ACM MobiCom* (2022).

[29] LI, S., ZHENG, H., ZHANG, C., SONG, Y., YANG, S., CHEN, M., LU, L., AND LI, M. Passive DSSS: Empowering the Downlink Communication for Backscatter Systems. In *Proc. of USENIX NSDI* (Apr. 2022), pp. 913–928.

[30] LI, Z., CHEN, B., YANG, Z., LI, H., XU, C., CHEN, X., WANG, K., AND XU, W. FerroTag: A Paper-Based MmWave-Scannable Tagging Infrastructure. In *Proc. of ACM SenSys* (2019), p. 324–337.

[31] LIANG, Q., DURRANI, T. S., GU, X., KOH, J., LI, Y., AND WANG, X. Guest Editorial Special Issue on Spectrum and Energy Efficient Communications for Internet of Things. *IEEE Internet of Things Journal 6*, 4 (2019), 5948–5953.

[32] LIU, J., JACKSON, D. R., AND LONG, Y. Substrate integrated waveguide (SIW) Leaky-Wave Antenna with Transverse Slots. *IEEE Transactions on Antennas and Propagation 60*, 1 (2011), 20–29.

[33] LIU, V., PARKS, A., TALLA, V., GOLLAKOTA, S., WETHERALL, D., AND SMITH, J. R. Ambient backscatter: Wireless communication out of thin air. *ACM SIGCOMM Computer Communication Review 43*, 4 (2013), 39–50.

[34] LIU, W., HUANG, K., ZHOU, X., AND DURRANI, S. Next Generation Backscatter Communication: Systems, Techniques, and Applications. *EURASIP Journal on Wireless Communications and Networking 2019*, 1 (2019), 1–11.

[35] LONG, S., AND MIAO, F. Research on ZigBee Wireless Communication Technology and its Application. In *IEEE IAEAC* (2019), vol. 1, pp. 1830–1834.

[36] LUETH, K. L. State of the IoT 2020: 12 billion IoT Connections, Surpassing Non-IoT for the First Time. Available at https://iot-analytics.com/state-of-the-iot-2020-12-billion-iot-connections-surpassing-non-iot-for-the-first-time/, 2020.

[37] MAZAHERI, M. H., CHEN, A., AND ABARI, O. MmTag: A Millimeter Wave Backscatter Network. In *Proc. of ACM SIGCOMM* (2021), p. 463–474.

[38] MIRRORCLE. MEMS Mirrors - Mirrorcle Technologies Inc. Available at https://www.mirrorcletech.com/wp/products/mems-mirrors/ (2022/04/20), 2022.

[39] MITTENDORFF, M., LI, S., AND MURPHY, T. E. Graphene-based Waveguide-Integrated Terahertz Modulator. *ACS Photonics 4*, 2 (2017), 316–321.

[40] NADERIPARIZI, S., HESSAR, M., TALLA, V., GOLLAKOTA, S., AND SMITH, J. R. Towards Battery-free HD Video Streaming. In *Proc. of USENIX NSDI* (2018), pp. 233–247.

[41] PENG, Y., SHANGGUAN, L., HU, Y., QIAN, Y., LIN, X., CHEN, X., FANG, D., AND JAMIESON, K. PLoRa: A Passive Long-Range Data Network from Ambient LoRa Transmissions. In *Proc. of ACM SIGCOMM* (2018), pp. 147–160.

[42] PETROV, V., KURNER, T., AND HOSAKO, I. IEEE 802.15.3d: First Standardization Efforts for Sub-Terahertz Band Communications toward 6G. *Comm. Mag. 58*, 11 (Nov 2020), 28–33.

[43] POLEMI, A., AND MACI, S. On the Polarization Properties of a Dielectric Leaky Wave Antenna. *IEEE Antennas and Wireless Propagation Letters 5* (2006), 306–310.

[44] PRADHAN, S., CHAI, E., SUNDARESAN, K., QIU, L., KHOJASTEPOUR, M. A., AND RANGARAJAN, S. Rio: A Pervasive RFID-based Touch Gesture Interface. In *Proc. of ACM MobiCom* (2017), pp. 261–274.

[45] QIN, Z., LI, F. Y., LI, G. Y., MCCANN, J. A., AND NI, Q. Low-power Wide-area Networks for Sustainable IoT. *IEEE Wireless communications 26*, 3 (2019), 140–145.

[46] RANGAN, S., RAPPAPORT, T. S., AND ERKIP, E. Millimeter-Wave Cellular Wireless Networks: Potentials and Challenges. *Proceedings of the IEEE 102*, 3 (2014), 366–385.

[47] RAPPAPORT, T. S., HEATH JR, R. W., DANIELS, R. C., AND MURDOCK, J. N. *Millimeter Wave Wireless Communications*. Pearson Education, 2015.

[48] RAPPAPORT, T. S., SUN, S., MAYZUS, R., ZHAO, H., AZAR, Y., WANG, K., WONG, G. N., SCHULZ, J. K., SAMIMI, M., AND GUTIERREZ, F. Millimeter Wave Mobile Communications for 5G Cellular: It Will Work! *IEEE Access 1* (2013), 335–349.

[49] REYNAERT, P., STEYAERT, W., STANDAERT, A., SIMIC, D., AND KAIZHE, G. mm-Wave and THz Circuit Design in Standard CMOS Technologies: Challenges and Opportunities. In *IEEE Asia Pacific Microwave Conference* (2017), pp. 85–88.

[50] SAEIDI, H., VENKATESH, S., LU, X., AND SENGUPTA, K. 22.1 THz Prism: One-Shot Simultaneous Multi-Node Angular Localization Using Spectrum-to-Space Mapping with 360-to-400GHz Broadband Transceiver and Dual-Port Integrated Leaky-Wave Antennas. In *IEEE International Solid- State Circuits Conference (ISSCC)* (2021), vol. 64, pp. 314–316.

[51] SENGUPTA, K., AND HAJIMIRI, A. A 0.28 THz Power-Generation and Beam-Steering Array in CMOS Based on Distributed Active Radiators. *IEEE Journal of Solid-State Circuits 47*, 12 (2012), 3013–3031.

[52] SKRIMPONIS, P., DUTTA, S., MEZZAVILLA, M., RANGAN, S., MIRFARSHBAFAN, S. H., STUDER, C., BUCKWALTER, J., AND RODWELL, M. Power Consumption Analysis for Mobile mmWave and Sub-THz Receivers. In *6G Wireless Summit* (2020), IEEE, pp. 1–5.

[53] SOLTANAGHAEI, E., PRABHAKARA, A., BALANUTA, A., ANDERSON, M., RABAEY, J. M., KUMAR, S., AND ROWE, A. Millimetro: MmWave Retro-Reflective Tags for Accurate, Long Range Localization. In *Proc. of ACM MobiCom* (2021), p. 69–82.

[54] SORNIN, N., LUIS, M., EIRICH, T., KRAMP, T., AND HERSENT, O. LoRaWAN Specifications, LoRa Alliance, San Ramon.

[55] SUTINJO, A., OKONIEWSKI, M., AND JOHNSTON, R. H. Radiation from fast and slow traveling waves. *IEEE Antennas and Propagation Magazine 50*, 4 (2008), 175–181.

[56] TALLA, V., HESSAR, M., KELLOGG, B., NAJAFI, A., SMITH, J. R., AND GOLLAKOTA, S. Lora Backscatter: Enabling the vision of Ubiquitous Connectivity. In *Proc. of ACM IMWUT* (2017), vol. 1, pp. 1–24.

[57] TONG, X., ZHU, F., WAN, Y., TIAN, X., AND WANG, X. Batch Localization Based on OFDMA backscatter. In *Proc. of the ACM IMWUT* (2019), vol. 3, pp. 1–25.

[58] WANG, Q., YU, J., XIONG, C., ZHAO, J., CHEN, S., ZHANG, R., AND GONG, W. Efficient Backscatter with Ambient WiFi for Live Streaming. In *IEEE Global Communications Conference* (2020), pp. 1–6.

[59] Y. YANG, M. MANDEHGAR, AND D. R. GRISCHKOWSKY. THz-TDS Characterization of the Digital Communication Channels of the Atmosphere and the Enabled Applications. *Journal of Infrared, Millimeter, and Terahertz Waves 36*, 1 (2015), 97–129.

[60] YANG, Y., MANDEHGAR, M., AND GRISCHKOWSKY, D. R. Understanding THz Pulse Propagation in the Atmosphere. *IEEE Transactions on Terahertz Science and Technology 2*, 4 (2012), 406–415.

[61] YEH, C.-Y., GHASEMPOUR, Y., AMARASINGHE, Y., MITTLEMAN, D. M., AND KNIGHTLY, E. W. Security in Terahertz WLANs with Leaky Wave Antennas. In *Proc. of ACM WiSec* (2020), pp. 317–327.

[62] ZHANG, J., SOLTANAGHAI, E., BALANUTA, A., GRIMSLEY, R., KUMAR, S., AND ROWE, A. PLatter: On the Feasibility of Building-Scale Power Line Backscatter. In *Proc. of USENIX NSDI 22* (Apr. 2022), pp. 897–911.